

Interferometry of Radiation Intensity of CW Gas Lasers

A. G. ARUTYUNYAN, S. A. AKHMANOV, V. G. TUNKIN, and A. S. CHIRKIN

Moscow State University

Submitted 5 August 1971

Zh. Eksp. Teor. Fiz. 62, 70-80, (January, 1972)

The results of measuring the intensity correlation function (ICF) $G^{(2)}(\tau)$ of a low-power He-Ne gas laser (emission wavelength of 1.15μ) are presented. A Michelson interferometer and a frequency doubler (OO \rightarrow E interaction) are used. Spatial and time ICF of nonlocked and locked axial modes are measured. Second harmonic was generated in a LiNbO₃ crystal both in the case of a 90° match and in the presence of birefringence. A theory of intensity interferometer that accounts simultaneously for time and spatial structure of laser emission is developed to interpret the experimental results. The effect of incomplete spatial beam coherence in the presence of birefringence on the results of measuring time ICF is considered. Time ICF for the measured inter-mode intensity distribution is computed. Comparison of the latter with experimental data shows that there is no mode phase correlation in non-locked operation and an incomplete phase correlation is observed in mode-locked operation. In the last case the contrasts of the $G^{(2)}(\tau)$ function correspond to the following values of the track contrast R for the two-photon technique: measured R = 2.1 and computed for completely mode-locked operation R = 2.8.

INTRODUCTION

INTENSITY interferometry, first successfully used by Hanbury Brown and Twiss in stellar interferometers^[1], is widely applied to study laser emission.

While the measurement of intensity correlation functions (ICF) of emissions with Gaussian statistics yields essentially the same information as the measurement of field correlation functions and the stimulus to study ICF is mainly due to technical advantages (elimination of phase fluctuations, increased resolution of narrow lines), ICF of non-Gaussian fields (laser emission is one of the most important examples of these) provides additional information on the envelope statistics.

Precisely because of this consideration the measurement of time ICF became widespread in the study of envelope statistics of multimode pulse lasers employing glass and ruby^[2-7] and of semiconductor pulse lasers^[8-10]. The cited papers show that time ICF yield important information on the mode phase statistics, time sequence of excitation of various modes, etc. Similar processes are of considerable interest also to other types of lasers, in particular low-power cw gas lasers. However, relatively little has been done in this area so far; only Davidson et al.^[11,12] report on the measurement of time ICF for a two-mode gas laser and its second harmonic. This case however is not very interesting since the phase statistics of two modes does not affect the ICF.

The purpose of this paper is a detailed investigation of ICF of low-power multimode cw lasers operating in various regimes (free running and axial mode locking). ICF was measured with the aid of frequency doubling; both time and spatial ICF were measured. In the study of time ICF considerable attention was paid to the effect of mode amplitude distribution on ICF^[1] and the effect of incomplete spatial beam coherence on the measurement results. The last problem was recently considered

in^[14] in connection with the two-photon technique of ICF measurement^[2].

1. FREQUENCY DOUBLING METHODS OF MEASURING THE INTENSITY CORRELATION FUNCTION (ICF)

The two-photon technique^[5-7] is the main method of measuring ICF in high-power pulse lasers. For measuring ICF in relatively low-power cw lasers, only frequency doublers are suitable^[8-10]. One such ICF measuring system is represented by a frequency doubler in which the mixed ordinary O and extraordinary E rays generate a second harmonic extraordinary ray E (OE-E interaction). In this system the mean intensity $\langle I \rangle$ of the second harmonic excited in a quasistationary regime directly yields the ICF of the fundamental emission

$$\langle I(t) \rangle \sim \langle I_1 I_2 \rangle = \langle I_1(t) I_2(t + \tau) \rangle = G^{(2)}(\tau). \tag{1}$$

Here I_1 and I_2 are the beam intensities of the fundamental emission and τ is the delay time between the beams, while the angle brackets denote averaging over the observation time. Another variant of ICF measurement based on second harmonic generation is represented by the OO-E interaction type. In this case the mean intensity of the harmonic is^[3]

$$\begin{aligned} \langle I \rangle \sim \langle I_1^2 \rangle + \langle I_2^2 \rangle + 4G^{(2)}(\tau) + 4 \operatorname{Re} \langle I_1(t) I_2(t + \tau) \\ \times A_1(t) A_2^*(t + \tau) \rangle e^{i\omega\tau} \\ + 2 \operatorname{Re} \langle A_1^2(t) A_2^{*2}(t + \tau) \rangle e^{2i\omega\tau}, \end{aligned} \tag{2}$$

where $A_i(t)$ are complex amplitudes and ω is the mean frequency of the fundamental emission.

Consequently, in addition to ICF $G^{(2)}(\tau)$, Eq. (2) contains other correlation functions of the fundamental emission field above the first order. All these correlation functions can be found in principle by measuring $\langle I \rangle$ as a function of τ .

The correlation function $\langle A_1^2(t) A_1^{*2}(t + \tau) \rangle$ must be

²An essentially analogous problem of the effect of spatial coherence on the results of experiments with photoelectric mixing of light beams was previously considered by Forrester et al. [15].

³The same expression determines the current of a two-quantum detector recording the Young interference pattern [16].

¹Time ICF are computed in the literature [13] only for a large number of modes with uniform and Gaussian amplitude distribution, i.e., for the case of solid-state lasers.

known, for example, to analyze the nonstationary regime of frequency doubling^[17]. From now on we are mainly interested in the function $G^{(2)}(\tau)$; it can be readily determined by averaging (2)⁴ over time τ within the limits $2\pi/\omega \ll \tau \ll \tau_c$, where τ_c is the shortest of the amplitude and phase correlation times. The averaging eliminates the last two terms from (2). The value of $\langle I_1^2 \rangle$ or $\langle I_2^2 \rangle$ is determined in the absence of one of the main beams. Therefore the function $G^{(2)}(\tau)$ can be readily normalized in a frequency doubler of this type. An additional control doubler is necessary for this purpose in the intensity correlator based on the OE-E interaction.

Equations (1) and (2) are written for plane waves. Correct analysis of experimental data requires a generalization of these equations to the case of spatial structure of laser beams. Furthermore we must consider the problem of the possible effect of birefringence of the nonlinear crystal on the measurement results. In order to compare the experimental results with theory we only attempt a theoretical analysis of an intensity correlator based on frequency doubling in the OO-E interaction.

2. SPACE-TIME ICF. THEORY.

For the above interaction type the complex amplitude of second harmonic field intensity in the approximation of a given field and geometric optics is given by the expression (see (20) in^[17])

$$A(x, y, t, z) = -i\tilde{\gamma} \int_0^z A_0^2 \left(x - \beta\xi, y, t - \frac{z}{u} \right) d\xi. \quad (3)$$

Here $\tilde{\gamma}$ is a nonlinear coefficient, $A_0(\mathbf{r}, t)$ is the amplitude of fundamental emission that consists of two beams, so that

$$A_0(\mathbf{r}, t) = A_1(\mathbf{r}, t) + A_2(\mathbf{r} - \rho, t + \tau) e^{i\omega\tau}, \quad (4)$$

and ρ is the distance between beam centers. In (3) the z axis is the direction of wave propagation (phase matching direction) and β is the birefringence angle of the harmonic wave. The velocities of the interacting waves are assumed equal, which is valid for lengths z much smaller than the quasi-static line L_q ^[17] ($L_q = 500$ cm for an LiNbO_3 crystal and gas laser emission at $\lambda = 1.15 \mu$).

An expression for the harmonic energy measured in the experiment can be obtained from (3) taking (4) into account

$$W_\tau = \frac{c}{8\pi} \oint ds \int (|A^2(x, y, t, z)|) dt, \quad (5)$$

where the index τ denotes averaging over τ ($\tau_c \gg \tau \gg 2\pi/\omega$). Integration over the area $ds = dx dy$ is performed in the plane of the photocathode. The structure of the quantity W_τ is analogous to the structure of $\langle I \rangle$ (2):

$$W_\tau = W_{11} + W_{22} + 4W_{12}; \quad (6)$$

W_{jj} is the energy of the harmonic generated by a single beam. The value of W_{12} is determined by correlation

properties of the fundamental emission and is equal to

$$W_{12} = \gamma^2 \int dt \oint ds \int_0^z A_1(x - \beta\xi_1, y, t) A_1^*(x - \beta\xi_2, y, t) \times A_2(x - \rho_x - \beta\xi_1, y - \rho_y, t + \tau) A_2^*(x - \rho_x - \beta\xi_2, y - \rho_y, t + \tau) d\xi_1 d\xi_2, \quad (7)$$

where $\gamma^2 = c\tilde{\gamma}^2/8\pi$.

We assume that the amplitudes A_1 and A_2 can be represented in the form

$$A_i(\mathbf{r}, t) = A_i^r(\mathbf{r}, t) A_i^{ra}(\mathbf{r}, t). \quad (8)$$

The function $A_i^r(\mathbf{r}, t)$ describes regular modulation of emission while $A_i^{ra}(\mathbf{r}, t)$ represents a random Gaussian process. We then obtain for the statistically average value of W_{12}

$$\bar{W}_{12} = \gamma^2 G^{(2)}(\tau, \rho) \iint_0^z \{ b^2[(\xi_2 - \xi_1)] + b(\tau, \rho_x + \beta(\xi_2 - \xi_1), \rho_y) \times b(\tau, \rho_x - \beta(\xi_2 - \xi_1), \rho_y) \} d\xi_1 d\xi_2. \quad (9)$$

Here

$$G^{(2)}(\tau, \rho) = \int dt \oint I_1^r(\mathbf{r}, t) I_2^r(\mathbf{r} + \rho, t + \tau) ds \quad (10)$$

is the space-time ICF of regular modulation and $b(\tau, \rho)$ is the normalized autocorrelation function of random modulation ($b(\tau, \rho) = A_i^{ra}(\mathbf{r}, t) A_i^{ra*}(\mathbf{r} + \rho, t + \tau)$). The derivation of (9) was based on the assumption that the birefringence effect can be neglected for regular modulation. Setting in (9) $\rho = 0$, $\tau = 0$, and $i = j$ we obtain averaged values for W_{11} and W_{22} .

Thus for the statistical mean value of the harmonic energy \bar{W}_τ (5), considering the intensities of exciting beam as equal ($I_1^r = I_2^r$), we have

$$F = \bar{W}_\tau = 4\gamma^2 G^{(2)}(0, 0) \iint_0^z \{ b^2[\beta(\xi_2 - \xi_1)] + g(\tau, \rho) \times [b^2(\beta(\xi_2 - \xi_1)) + b(\tau, \rho_x + \beta(\xi_2 - \xi_1), \rho_y) b(\tau, \rho_x - \beta(\xi_2 - \xi_1), \rho_y)] \} d\xi_1 d\xi_2, \quad (11)$$

where

$$g(\tau, \rho) = G^{(2)}(\tau, \rho) / G^{(2)}(0, 0).$$

In the absence of the birefringence effect ($\beta = 0$) (11) assumes the form

$$F = 4(\gamma^2)^2 G^{(2)}(0, 0) \{ 1 + g(\tau, \rho) [1 + b^2(\tau, \rho)] \}. \quad (12)$$

The last term in (12) represents a space-time ICF of the initial beam that has both the regular and random modulations described by Gaussian statistics.

Equation (12) is applicable also to the two-photon technique and leads to results that were obtained in a somewhat different manner in^[14]. Indeed for beams with only the regular modulation ($b(\tau, \rho) = 1$)

$$F \sim \{ 1 + 2g(\tau, \rho) \}. \quad (13)$$

In the presence of random spatial modulation of the fundamental emission (13) is valid if the initial beams coincide completely ($\rho = 0$).

If the fundamental emission has random modulation and in addition a shift $\rho \gg r_c$ and (or) the delay time of the beams $\tau \gg \tau_c$ ($b(\tau, \rho) = 0$), then

$$F \sim \{ 1 + g(\tau, \rho) \}. \quad (14)$$

Comparing (13) and (14) we see that the contrast of the function $F(\tau, 0)$, i.e., the ratio $R = F_{\max}/F_{\min}$, significantly depends on the accuracy of coincidence of the initial beams. In particular for cases of laser emission with completely non-locked and locked axial modes (14)

⁴According to the two-photon technique, such averaging is due to the finite spatial resolution of photographic film^[13].

yields

$$R^{ne} = 1, \quad R^{me} = 2, \quad (15a)$$

instead of the well-known values obtained from (13)

$$R^{ne} = 1.5, \quad R^{me} = 3. \quad (15b)$$

In the presence of birefringence in the nonlinear crystal the contrast of time function $F(\tau)$ (11) generally depends both on the shift ρ and birefringence β . With an accurate coincidence of the main beams ($\rho = 0$) crystal birefringence affects only the absolute value of $F(\tau)$ without changing its contrast. A similar effect can also occur in the case of the Gaussian correlation function $b(\tau, \rho)$; then

$$F(\tau, \rho) \sim \{1 + g(\tau, \rho) [1 + b^2(\tau, \rho)]\} \int_0^z (z - \xi) b^2(\beta \xi) d\xi \quad (16)$$

and shift ρ plays precisely the same role as in the case $\beta = 0$.

Therefore correct analysis of time ICF requires that the interacting beams be completely coincident; it is also desirable that frequency doubling occur at a 90° match ($\beta = 0$).

We note that the above pertains to the OO-E interaction type. A similar analysis performed for the OE-E interaction type, i.e., generalization of (1) taking spatial beam modulation into account, shows that crystal birefringence lowers the contrast of the function $\langle I \rangle$.

We now compute some time ICF without considering spatial structure of laser emission. Complex amplitudes $A_1(t)$ and $A_2(t)$ of the beams are represented in the form

$$A_j(t) = \sum_{n=1}^N a_n \exp\{i[n\Omega t + \varphi_n(t)]\}, \quad (j = 1, 2), \quad (17)$$

where N is the number of modes of laser emission, a_{jn} and φ_n are mode amplitudes and phases, and Ω is the intermode beat frequency. For any number N simple formulas for the correlation function $g(\tau)$ can be obtained only if amplitudes are equal $a_{jn} = a_j$.

In the case of non-locked modes we obtain the following expression for $g(\tau)$ averaged over random phases φ_n :

$$g^{ne}(\tau) = \frac{1}{2} \left[1 + \frac{\sin^2(N\Omega\tau/2)}{(N^2 - N)\sin^2(\Omega\tau/2)} \right]. \quad (18)$$

The contrast of this function is

$$R_s^{ne} = \left(2 - \frac{1}{N} \right) / \left(1 - \frac{1}{N} \right); \quad (19)$$

its value is larger than 2 if N is small. For $N \rightarrow \infty$ the value of $R_s^{ne} \rightarrow 2$.

In the case of mode-locked emission we have for the function $g(\tau)$

$$g^{me}(\tau) = \frac{3}{N(2N^2 + 1)} \left\{ N^2 + 2 \sum_{j=1}^{N-1} (N-j)^2 \cos(j\Omega\tau) \right\}, \quad (20)$$

Here the contrast for odd N , for example, is

$$R_s^{me} = 1/3(2N^2 + 1). \quad (21)$$

The correlation functions $g(\tau)$ (18) and (20) are periodic with an intermode beat period of $\tau = 2\pi/\Omega$; they fall off significantly in time periods $\tau_c \approx \pi/[(N-1)\Omega]$. For $\pi \lesssim 2\Omega\tau \lesssim 3\pi$ function (18) has weak beats whose

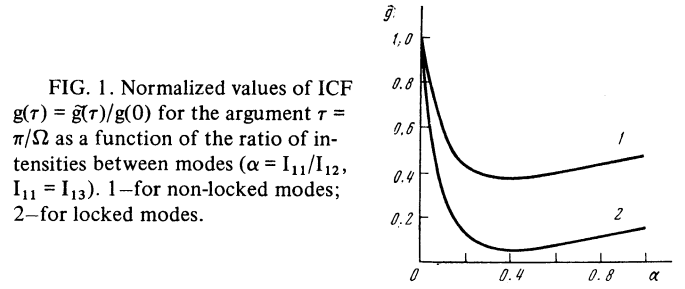


FIG. 1. Normalized values of ICF $g(\tau) = \tilde{g}(\tau)/g(0)$ for the argument $\tau = \pi/\Omega$ as a function of the ratio of intensities between modes ($\alpha = I_{11}/I_{12}$, $I_{11} = I_{13}$). 1—for non-locked modes; 2—for locked modes.

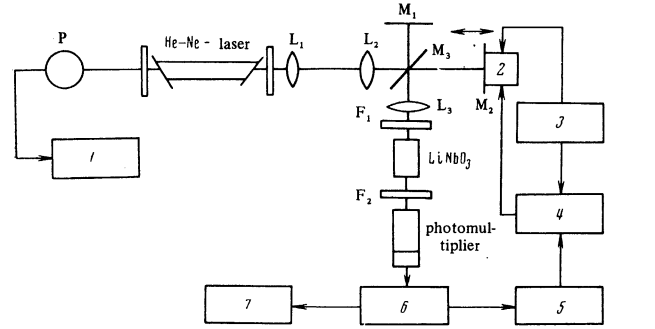


FIG. 2. Diagram of experimental setup for the measurement of ICF of laser emission by means of second harmonic generation. $M_{1,2,3}$ —mirrors; L_1, L_2, L_3 —lenses with focal lengths 2, 8, 12 cm respectively; F_1 —IKS-3 filter; F_2 —SZS-14 filter; P—photodiode; 1—spectrum analyzer; 2—piezoceramic; 3—sound generator; 4—self-tuning system; 5—expander, detector; 6—shaper; 7—counter.

depth decreases with increased N and is less for non-uniform distribution of mode amplitudes. The number of maxima in the indicated segment $\Omega\tau$ is $(N-2)$. The behavior of the function $g^{ml}(\tau)$ (20) is more monotonic than that of $g^{nl}(\tau)$.

The contrasts (19) and (21) are obtained for equal mode amplitudes; generally speaking they strongly depend on the distribution of laser emission intensity among the modes. This is illustrated by curves in Fig. 1 plotted for three-mode emission with a symmetric spectrum.

3. THE EXPERIMENTAL SETUP

The diagram of the setup for measuring ICF is shown in Fig. 2. A He-Ne laser operating at the wavelength 1.15μ was used as the source of the investigated emission. A Michelson interferometer formed by mirrors M_1 and M_2 and semitransparent mirror M_3 was used to split the emission into two beams and to introduce a delay between them. Mirror M_2 was free to move through 1 m along the optical bench and finer displacement through several μ was obtained with a piezoceramic mount attached to the mirror. The varying degree of coincidence of the beams at interferometer output was obtained with mirror M_2 regulated by micrometer feed with piezoceramic plates. The alignment accuracy of mirrors M_1 and M_2 was checked either by the power of the second harmonic (a sawtooth voltage was delivered to mirror M_2 piezoceramic to average the interference pattern over time τ) or more precisely by the maximum of the interference pattern to which the system was tuned by means of a self-tuning arrangement described below. Alignment was performed at

each point of measurement of the correlation function. To reduce angular divergence of the beams a telescope broadening the beam diameter by a factor of four was placed in front of the interferometer. A Nicol prism and a quarter-wave plate decoupled the laser from the interferometer. Mode locking was checked with the aid of a fast acting photodiode and spectrum analyzer showing the intermode beats signal. A scanning interferometer measured the intensity distribution among the modes.

The emission emerging of the Michelson interferometer was focused into a LiNbO₃ crystal oriented in the phase match direction to generate the second harmonic in the OO-E interaction. The harmonic was recorded by a photomultiplier operating in the photon counting regime. The pulse output of the photomultiplier was connected to the counter. The same pulses entered the pulse expander and detector. The signal of the detector was fed directly to the self-tuning system that included a synchronous detector. The self-tuning system operated by impressing a small 30 Hz ac voltage on the ceramic mount of mirror M₂; the same voltage served as reference voltage in the synchronous detector. The error signal from the self-tuning output was fed to the piezoceramic mount of mirror M₂. This tuned the system to the maximum or minimum of interference pattern (2). The self-tuning arrangement was used also during alignment of the optical system.

4. EXPERIMENTAL RESULTS. DISCUSSION

Using the above setup we measured spatial and time ICF of the He-Ne laser. In the measurement of spatial ICF the time delay between the beams $\tau = 0$. The nonlinear LiNbO₃ crystal was either at room temperature (the phase matching angle for the OO-E interaction is 66° 30', birefringence $\beta \neq 0$) or at the 90° match angle temperature ($t^\circ \approx 220^\circ \text{C}$, $\beta = 0$). The laser operated in the fundamental transverse mode or in a free-running regime exciting only one or several modes of high order (approximately the tenth order). The form of the spatial correlation functions was approximately the same in all cases; Fig. 3 shows the ICF for one case. The coherence radius was usually determined by beam radius in the cases under study. This is apparently due to the generation of a single mode or a small number of transverse modes. This consideration does not permit

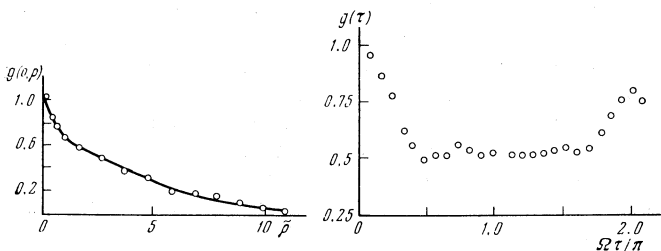


FIG. 3

FIG. 3. Transverse spatial ICF of He-Ne laser operating with several transverse modes; measurements made for 90° match angle in nonlinear crystal. Circles are experimental values; \tilde{p} is beam shift in arbitrary units.

FIG. 4. Time ICF of He-Ne laser operating with several axial and transverse modes; $\Omega\tau = 2\pi l/L$; Ω —intermode beats frequency; L —length of laser resonator; l —difference between interferometer arms.

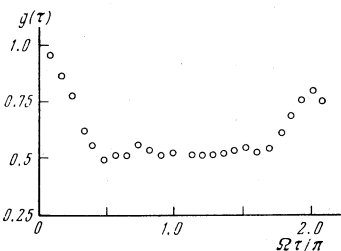


FIG. 4

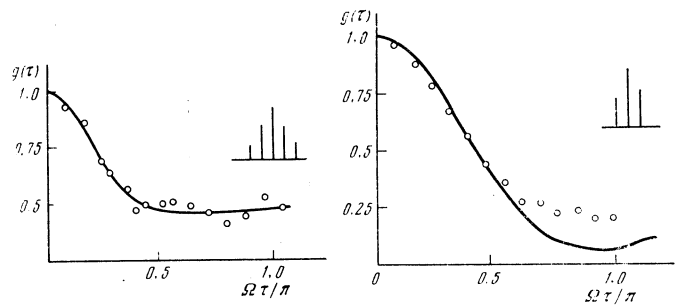


FIG. 5

FIG. 6

FIG. 5. Time ICF of He-Ne laser with non-locked modes; number of modes $N = 5$. Circles are experimental values; theoretical curve plotted for intermode intensity distribution of 0.26:0.61:1:0.61:0.26.

FIG. 6. Time ICF of He-Ne laser for self-locked modes; number of modes $N = 3$. Circles are experimental values; theoretical curve plotted for intermode intensity distribution of 0.63:1:0.48.

us to assume confidently that birefringence does not affect ICF, although the experimental data do not contradict such a conclusion.

We used spatial ICF to determine the alignment of mirrors M₁ and M₂. The value of the function

$$g^{(2)}(\tau) + G^{(2)}(\tau) / (\langle I_1^2 \rangle \langle I_2^2 \rangle)^{1/2} = 1$$

for $\tau = 0$ indicates the coincidence of coherence regions of the beams exciting the second harmonic.

The operation of the entire system was checked by measuring the time ICF for the case of two or three transverse and several axial modes (see Fig. 4). The drop in function $g(\tau)$ is approximately equal to two which indicates that the field statistic is close to Gaussian. A second maximum less than unity appears in $g(\tau)$ for delay lengths $l = 2\pi c/\Omega$ (in our case $\Omega/2\pi = 150 \text{ MHz}$ and $l \approx 100 \text{ cm}$). This effect seems to be due to the deteriorating coincidence of the fundamental beams when l is large because of angular divergence. Another cause of this effect could be the finite width $\Delta\omega$ in the spectrum of an individual mode. However according to data reported in the literature (for example in^[18,19]) this width $\lesssim 10^4 \text{ Hz}$. Therefore phase fluctuations can be neglected for lengths $l \approx 100 \text{ cm}$ ($l\Delta\omega/c \sim 10^{-4}$). Therefore there is no drop in the function $g(\tau)$ due to finite time of phase correlation. We performed the successive measurements for delay lengths l up to 50 cm.

Figures 5 and 6 show the measured time ICF of lasers with non-locked and self-locked axial modes. The same figures show ICF computed for the measured intermode intensity distribution. For the case of non-locked modes the experimental points coincide with the theoretical curve in a satisfactory manner, and are above the theoretical curve for the case of self-locked modes. Minimal values of $g^{ml}(\tau)$ are 0.20 for the experimental case and 0.07 for the theoretical one. Converted to the contrast in the two-photon technique, this corresponds to the measured value $R = 2.14$ and to the expected value $R = 2.77$ for the given mode intensity distribution. The obtained difference is larger than the possible experimental error.

The accuracy with which we measured experimental

values was about 1%. Therefore the computational error is important in the comparison of experimental and theoretical values. The principal error here is due to the inaccuracy of determination of mode intensities; in our case it amounted to $\sim 10\%$. At the same time curve 2 in Fig. 1 shows that the minimum value of $g(\tau)$ does not exceed 0.10 even for a 20% error. Consequently the lack of coincidence between experimental values and the theoretical curve in Fig. 6 is due to incomplete mode locking. We note that incomplete mode locking in the He-Ne laser in the self-locking regime was observed also in other cases (for example in^[20]); only Smith^[21] reports a complete self-locking.

CONCLUSION

The reported investigation thus shows that intensity interferometers based on second harmonic generation can be successfully applied to analyze the operation of low-power gas lasers. Such a nonlinear interferometer can be used to measure both the time and spatial ICF.

The resolution time τ_{res} of nonlinear interferometers is determined by group delay effects involving waves interacting in the nonlinear crystal. For the interferometer type considered here $\tau_{\text{res}} = \nu z$, where $\nu = 1/u_{2\omega} - 1/u_{\omega}$, u_{Ω} is the group velocity at the corresponding frequency, and z is the length of the crystal. The harmonic excitation process is quasistatic ("inertialess") for correlation time $\tau_c > \tau_{\text{res}}$ of the fundamental emission. For KDP and LiNbO₃ crystals with $z = 1$ cm and for the fundamental wavelength of $\lambda \approx 1 \mu$ τ_{res} equals 10^{-13} and 5×10^{-12} sec respectively which is 10^4 – 10^2 times less than the resolution time of the Brown-Twiss interferometer.

The finite spatial resolution r_{res} of the nonlinear interferometer is due to birefringence β of the crystal affecting the extraordinary harmonic ray: $r_{\text{res}} = \beta z$. A typical value of $r_{\text{res}} \approx 3 \times 10^{-2}$ cm for $z = 1$ and can be much less than this value for a phase match angle near 90° .

We can readily see that the values of τ_{res} and r_{res} can be changed significantly by varying the length of the crystal. Because of this nonlinear crystal interferometers can be used in the interferometry of conventional non-laser sources with a broad frequency and angular spectrum.

A disadvantage of the above interferometer is the small coefficient of transformation in the analysis of weak fields requiring highly sensitive detectors. To increase the coefficient of nonlinear transformation we can however use methods in which the transformation process is accompanied by amplification.

We note that instead of measuring ICF we can obtain data on intermode phase relationships by measuring the statistics of photon counts for the second harmonic^[22]. However in the general case it is not possible to compare the results of intensity interferometry with harmonic photon statistics since the latter depends not only on the ICF $G^{(2)}(\tau)$ but also on higher order functions. In particular the dispersion of photon counts of the harmonic depends on fourth order ICF. Such a comparison can thus be performed only for non-locked modes. Computation shows that in the situation corresponding to Fig. 5 the value of d measured in the experiment^[22] should be equal to 0.26. At the same time according to^[22] the experimental value $d = 0.13$; we attributed this to a partial mode locking.

The authors are indebted to A. V. Grigor'ev for aid in preparing the experimental setup.

¹R. Hanbury Brown and R. Twiss, *Nature* 177, 27 (1956).

²J. A. Armstrong, *Appl. Phys. Lett.* 10, 16 (1967).

³J. Klauder, M. Duguay, J. Giordmaine, and S. Shapiro, *Appl. Phys. Lett.* 13, 174 (1968).

⁴S. A. Akhmanov and A. S. Chirkin, *IVUZ Radiofizika* 13, 787 (1970).

⁵A. J. DeMaria, W. H. Glenn, M. J. Brienza, and M. E. Mack, *Proc. IEEE* 57, 2 (1969).

⁶R. Dändliker and H. P. Weber, *Z. angew. Phys.* 29, 90 (1970).

⁷M. A. Duguay, J. M. Hansen, and S. L. Shapiro, *IEEE J. Quant. Electron.* 6, 725 (1970).

⁸D. Gloge and R. Roldan, *Appl. Phys. Lett.* 14, 3 (1969).

⁹H. P. Weber and D. Gloge, *Appl. Phys. Lett.* 17, 231 (1970).

¹⁰D. Gloge and T. P. Lee, *IEEE J. Quant. Electron.* 7, 43 (1971).

¹¹F. Davidson, J. Klebba, C. Laurence, and F. Tittel, *Appl. Phys. Lett.* 17, 117 (1970).

¹²F. Tittel, J. Klebba, and F. Davidson, *Appl. Optics* 10, 213 (1971).

¹³H. E. Rowe and T. Li, *IEEE J. Quant. Electron.* 6, 49 (1970).

¹⁴H. Weber and H. G. Danielmeyer, *Phys. Rev. A* 2, 2074 (1970).

¹⁵A. T. Forrester, H. A. Gudmundsen, and P. O. Iohson, *Phys. Rev.* 99, 1691 (1955).

¹⁶P. P. Barashev, *Phys. Lett.* 32A, 291 (1970).

¹⁷S. A. Akhmanov, A. I. Kovrigin, A. S. Chirkin, O. N. Chunaev, *Zh. Eksp. Teor. Fiz.* 50, 829 (1966) [*Sov. Phys. JETP* 23, 549 (1966)].

¹⁸A. Javan, W. R. Bennett, Jr., and D. R. Herriot, *Phys. Rev. Lett.* 6, 106 (1961).

¹⁹Yu. I. Zaitsev and D. P. Stepanov, *Zh. Eksp. Teor. Fiz.* 55, 1645 (1968) [*Sov. Phys. JETP* 28, 863 (1969)].

²⁰A. Frova, M. A. Duguay, C. G. B. Garrett, and S. L. McCall, *J. Appl. Phys.* 40, 3969 (1969).

²¹P. W. Smith, *Optics Comm.* 2, 292 (1970).

²²S. A. Akhmanov, A. S. Chirkin, and V. G. Tunkin, *Opto-Electron.* 1, 196 (1969).